Impact of the crystal structure of HfO_2 on the transport properties of model $HfO_2/Si/HfO_2$ silicon-on-insulator field-effect transistors: A combined DFT-scattering theory approach

G. Giorgi*
Department of Chemical System Engineering, Graduate School of Engineering, The University of Tokyo, Tokyo 113-8656, Japan and Department of Chemistry and CNR-ISTM, Università di Perugia, via Elce di Sotto, 8, I-06123 Perugia, Italy

L. R. C. Fonseca†
Wernher von Braun Center for Advanced Research, Av. Alice CPN Mattosinho 301, Campinas, SP 13098-392, Brazil

A. Korkin‡
Nano and Giga Solutions, Gilbert, Arizona 85296, USA

K. Yamashita§
Department of Chemical System Engineering, Graduate School of Engineering, The University of Tokyo, Tokyo 113-8656, Japan
(Received 3 January 2009; revised manuscript received 28 April 2009; published 4 June 2009)

Motivated by the polycrystalline structure of the high permittivity dielectric HfO_2 in contact with Si, we report calculations of carrier transport in nanometer-thin atomistic silicon-on-insulator field-effect transistor models. To qualitatively understand the impact of different crystalline phases of the dielectric on the transport characteristics of the channel, we have investigated two polymorphs of HfO_2 interfacing with Si, namely, the well-known tetragonal (t-HfO_2) and the theoretically proposed anatase (a-HfO_2) phases. For the transport calculations we have employed tetragonal-(t-HfO_2/Si/t-HfO_2) and anatase-based (a-HfO_2/Si/a-HfO_2) NSOI films. Our calculations reveal that transport is more efficient for the anatase polymorph since its good lattice match to Si does not create interface states in the Si band gap. The tetragonal polymorph creates scattering states in the Si band valence-band edge through the presence of stretched Si-Si bonds at the interface, resulting in degraded transport characteristics. Our study suggests that different bonding arrangements along the channel length create regions of increased carrier scattering even in the absence of other scattering processes such as phonons, trapped charges, or interface roughness.

DOI: 10.1103/PhysRevB.79.235308 PACS number(s): 73.40.−c, 73.20.−r, 71.20.−b

I. INTRODUCTION

Even if 30 years have passed since the introduction of the silicon-on-insulator (SOI) technology, nowadays it still represents one of the few, if not the only, practical alternatives to bulk silicon for ultradense integrated circuit building in the foreseeable future.[1] In particular, Si and SiO_2 have embodied for several decades the "ideal" semiconductor-dielectric pair in bulk and SOI microelectronics engineering. The similar chemical nature of their covalent bonds, in addition to the superior manufacturing qualities of silica leading to a low density of the bulk and interface defects, have made these two materials the most suitable for transistor and integrated circuit (IC) building until now. Indeed, modern device requirements of low cost, compactness, speed, and low power are shifting the traditional technology of semiconductors from the microscopic to the nanoscopic scale. As a result, we are now facing up to the attainment of several physical limits to further down-scale device dimensions as predicted by Moore's empirical law.[2] In particular, the silica thickness has reached its limit in complementary oxide semiconductors (CMOSs), where going beyond the threshold value of about 1 nm highly reduces the silica dielectric properties, leading to high leakage currents following direct tunneling across the oxide and to the difficulties in achieving oxide thickness uniformity across the wafer. Thus, one of the most pressing challenges of material science in microelectronics is to find alternative gate insulators characterized by a dielectric constant (k) larger than that of SiO_2, allowing for thicker oxide slabs (thus lower leakage current) but with the same equivalent oxide thickness (thus the same oxide capacitance), while maintaining the same excellent electrical characteristics of SiO_2.

A large number of high-k compounds have been suggested (Al_2O_3, La_2O_3, Y_2O_3, MgO, CaO, $ZrSiO_4$, $HfSiO_4$, HfO_2, ZrO_2, TiO_2, and many others). However, the difference in the nature of the Si-Si (covalent) and M-O (ionic) bonds can enhance defect formation at the interface and in the bulk of the dielectric, affecting device performance. A fundamental peculiarity of silica is its thermodynamic stability on Si, i.e., its ability to withstand the high temperatures of the annealing processes, avoiding unwanted compound formation, such as silicides. According to this requirement, oxides and silicates of Hf and Zr seem to be the most promising among the dielectrics tested so far.[3] Hafnia, similar to zirconia, is characterized by three main crystalline polymorphs: monoclinic (m), tetragonal (t), and cubic (c). They undergo phase transition at ordinary pressure and increasing temperature,[4] according to

$$m\text{-}HfO_2(P2_1/c) \xrightarrow{1720\ ^\circ C} t\text{-}HfO_2(P4_2/nmc) \xrightarrow{2600\ ^\circ C} c\text{-}HfO_2(Fm3m).$$

Other crystalline polymorphs such as the orthorhombic

(*Pbca*) and the cotunnite (*Pnma*) phases are experimentally detected only at higher pressure.[5–9] Upon growth on Si and subsequent 1000 °C annealing steps typical in the field-effect transistor (FET) process,[10,11] HfO_2 adopts a polycrystalline structure, with the dominant presence of the monoclinic phase, even though traces of the tetragonal phase can be often detected.[12,13]

Due to their ceramic properties and potential technological applications, the electronic and structural properties of both ZrO_2 and HfO_2 have deserved wide analysis both experimentally and theoretically. Fiorentini and Gulleri employed the *ab initio* projected augmented wave (PAW) method to calculate the dielectric properties of both oxides,[14] concluding that except for the electron injection barriers which seem to be too small, they represent the only new and viable gate oxides. Foster *et al.* calculated the structural and electronic properties of both hafnia and zirconia using the plane wave (PW) method,[15,16] focusing on the effects of vacancies and interstitials. They concluded that the atomic interstitial incorporation of oxygen is preferred over the molecular and, in presence of electrons available from the Si conduction band (CB), charged defective species are more stable than neutral ones. In a study of ZrO_2 polymorphism, Dewhurst and Lowther[17] predicted the stability of all hypothetical high-pressure phases of zirconia, revealing the possible presence of a tetragonal-like structure whose symmetry point group ($I4_1/amd$) is exactly that of anatase, a polymorph of TiO_2. Its stability is intermediate between that of rutile (most stable and dense) and brookite. The authors suggested that for zirconia and hafnia, the anatase (*a*-) phase constitutes an exception since from the Birch equation of state it is lower in energy with respect to the other phases considered,[18] while its larger volume (+18% than that of *m*-ZrO_2) makes a *a*-ZrO_2 plausible crack retarder in the phase transition between *t*- and *m*-ZrO_2.

The replacement of SiO_2 by high-*k* oxides has carried over the knowledge accumulated in decades of research on the Si/SiO_2 interface to the Si/high-*k* interface.[19–22] Peacock *et al.*[23,24] investigated the effect of saturation of oxygen on a large variety of Si/MO_2 (M=Zr,Hf) interfaces, finding that the O-terminated ones have no gap states and also that the band offsets are independent of the interfacial bonding. Analysis of *t*-ZrO_2/Si and $ZrSiO_4$/Si by Puthenkovilakam *et al.*[25] concluded that the decrease in the coordination of Zr atoms with respect to the bulk values populates the Fermi level with Zr dangling bonds *d* states; to avoid the problem they suggested to saturate the dangling bonds with H and O atoms.

Si/SiO_2 interfaces have also been subject to extensive theoretical and experimental charge-carrier transport analysis to explain the effect of the interface and the bulk defects on the transport properties of the inversion layer. Theoretical methods such as the Monte Carlo approach,[26] the phenomenological models,[27] and the nonequilibrium Green's functions (NEGF) have been employed over the years.[28] The picture emerged from these studies indicates that the charge mobility in the channel depends on the transversal field, which sets different mechanisms for scattering: at low-transversal fields scattering is dominated by phonons in the dielectric, while at high fields it is the interface roughness the main cause of mobility degradation.[26] In addition, the bulk and the interface defects must be avoided through improved processing steps, including defect saturation by hydrogen and deuterium to maximize mobility.[29]

Double gate (DG)-FET devices share with SOI devices the same oxide/silicon/oxide geometry, but make use of one extra metal electrode buried below the bottom oxide to enhance electrostatic control over the silicon channel.[30] Si/SiO_2-based DG-FETs have been simulated to test new theoretical methodologies; the QDAME (quantum device analysis of modal evaluation) is an algorithm based on a novel hybrid Newton-Broyden technique whose capabilities have been demonstrated by calculating the role in surface roughness and contact geometry on the current degradation of Si/SiO_2 DG-FETs.[31] Recently Gnani *et al.*[32] reported a theoretical comparison between a DG-FET and a cylindrical nanowire FET using HfO_2 and SiO_2 as gate dielectrics and considering FETs with the same oxide thickness. They report a worsening of the short channel effect for HfO_2 compared to SiO_2, even if hafnia more than silica is able to improve the on current due to lateral capacitive-coupling effects, despite the degraded low-field mobility.

Combining the density-functional theory (DFT) (Ref. 33) and the nonperturbative scattering theory,[34] Fonseca *et al.*[35] focused on the tunneling across a symmetric $Si/HfO_2/Si$ double interface system and on the influence that point defects have on the leakage current. In particular, oxygen vacancies at the interfaces, similarly to interstitial boron atoms in the hafnia region, can introduce states in the Si band gap, meaning that even at low-gate bias the leakage current can be strongly affected by these two types of defects. Employing the same technique, Ribeiro *et al.*[36] recently investigated transport in the channel of a model nano-SOI (NSOI) based on SiO_2 in the presence of oxygen vacancies at the interface (Pb-like centers).[37–39] They found that even though hydrogen passivation of Si dangling bonds improves on the conductance of the channel with respect to the unpassivated interface, the conductance is still severely degraded from its theoretical maximum value, attained for an idealized, defect-free interface.

The polycrystalline structure of annealed HfO_2 on Si raises the question of the impact on the channel transport of the different crystal phases and orientations assumed by the grains in the dielectric. In this paper we calculate the transport characteristics of electrons and holes in two symmetric $HfO_2/Si/HfO_2$ NSOI geometries differing by the crystal structure of HfO_2. We employ DFT both at the PWs and the linear combination of atomic orbitals (LCAO) levels for structure relaxation and electronic structure calculation, combined with non-perturbative scattering theory for transport calculation.[35] We adopt the tetragonal and anatase crystal phases for the dielectric as models for the different grain structures and the corresponding interfaces. Our aim is to address qualitatively the question stated above since a large number of possible grain phases and orientations may occur in real systems, making a more detailed study at the current atomistic level impractical.

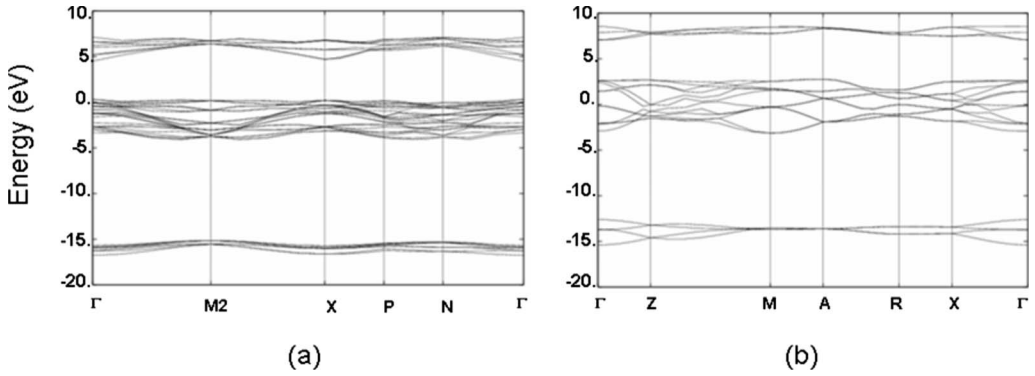

FIG. 1. Band structure of the (a) anatase and (b) tetragonal HfO_2 phases.

II. METHOD

A. Electronic structure calculation

We used DFT for atomic relaxation and electronic structure calculation, both at generalized gradient approximation (GGA) and local-density approximation (LDA) levels,[40–42] as implemented in Vienna *ab initio* simulation package (VASP).[43] Core electrons were replaced by ultrasoft pseudopotentials (USPP).[44,45] The Ceperley-Alder (CA) exchange-correlation potential was used within the LDA,[46] while Perdew-Wang 91 (PW91) was used within the GGA.[47–49] The PW basis set was truncated at 396 and 700 eV for augmentation charge cutoff. We employed a $4\times1\times4$ Monkhorst-Pack k-point grid to relax our initial interface structures (described below) until the maximum force was lower than 0.05 eV/Å.[50] Convergence of the residual forces was checked increasing the grid to $6\times1\times6$. A $6\times6\times6$ grid was used for the reference tetragonal and anatase (t- and a-HfO_2) bulk unit cells. Figure 1 shows the band structures for those polymorphs which are very similar, particularly the band gaps (4.3 and 4.2 eV, respectively).

Reference 51 describes in detail our model interfaces and discusses the possible coexistence of the well-established tetragonal phase and the hypothetical anatase phase of HfO_2 as they interface with Si (100). In that work the two phases of the refractory oxides MO_2 (M=Zr,Hf) were considered for the periodic double interface MO_2/Si, the closer match between the Si(100) and the a-MO_2 lattice vectors resulted in overall a-MO_2/Si supercells with a reduced amount of stress relative to t-MO_2/Si ones. Even though anatase MO_2 has not yet been measured, it has been proposed as a transition layer to explain the preferential orientation growth of monoclinic HfO_2 on Ge and on GaAs (Ref. 52) highlighting the relevance of this hypothetical phase. The oxygen-rich composition adopted for both interface models reflects the presence of a SiO_x interfacial layer grown under all MO deposition processes.

In the present work, we adopt the Si experimental cubic unit-cell vectors (a=3.8403 Å) as the in-plane fixed lattice parameters for interface building. This choice stems from the fact that since the oxide is deposited on top of Si it is expected that at least the first few monolayers of the oxide should adjust the Si unit cell. Besides, by keeping the Si lattice vectors fixed we are able to compare transport in the presence of different interfaces without the need to account for the complex relation between conductance and bulk strain in the channel. The ionic positions along the interfaces were optimized as explained below.

Our model NSOI were built as symmetric HfO_2/Si/HfO_2 structures (Fig. 2) made of 37 atoms in both tetragonal and anatase cases. The t- and a-HfO_2 slabs contain 3 Hf planes on each side of the interfaces and are terminated with H atoms. A vacuum gap ~30 Å thick separates the structures from their periodic images along the normal to the interfaces. The t- and a-slabs total thicknesses are 7.7 and 8.2 Å, approximately. Our slabs are very thin compared with those from the experiments, usually found in the range 20–30 Å. This choice stems from the need to control the number of atoms in the calculations. As described below in detail, to calculate the electronic current through the device the unit cell was multiplied by eight along the transport direction, resulting in structures containing 296 atoms. Increasing a larger number of atoms to allow for thicker oxides would

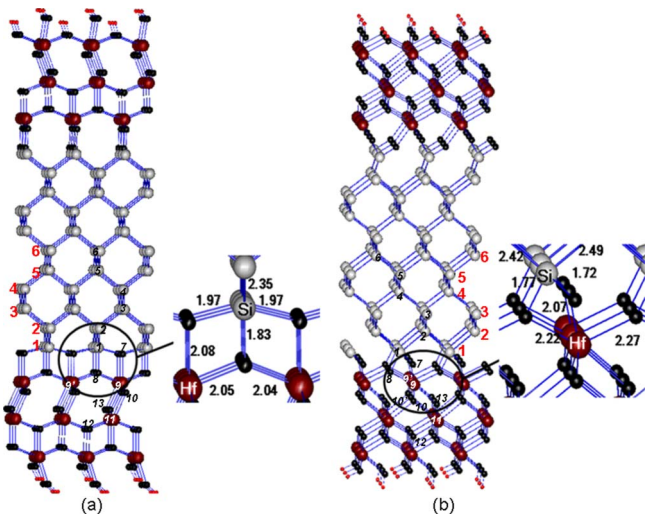

FIG. 2. (Color online) Enlarged (3×3) structures of our double symmetric (a) anatase-based a-HfO_2/Si/a-HfO_2 (a-NSOI) structures and (b) tetragonal-based t-HfO_2/Si/t-HfO_2 (t-NSOI). The insets show in detail the bonding configurations at the interfaces. Larger numbering indicates atomic layers and smaller numbering indicates individual atoms (intermediate white: Si; large gray: Hf; small black: O).

make our calculations impractical. Moreover, there would be a little change in our conclusions if thicker oxides had been used as the electron wave-function penetration in the oxide only extends for a few angstroms.

For both structures 11 Si atom planes (14.9 Å thick) form the channel. The Si growth direction is [100] while the transport direction is [011]. Such thickness is insufficient to avoid quantum effects due to the structural confinement. Indeed, our calculations indicate that the DFT Si band gap calculated in the middle of the Si slab is about 1.5 times larger than its bulk value. However, since our transport calculations (described below) are performed near the band edges the larger band gap does not impact our main conclusions. To mimic an ultra-thin interfacial layer (IL) between the dielectric and the Si channel, in both interfaces one monolayer of oxygen was added to obtain a Hf-O-Si interface bond configuration (half a monolayer added to each side of the interface), thus avoiding direct Si-Hf contact. All the O atoms at the exposed surfaces were saturated with H making them twofold coordinated.

Symmetry for the two interfaces in both *a*- and *t*-based NSOI was achieved through the combined operation of rotation about the axis perpendicular to the interfacial plane followed by reflection across the plane constituted by the sixth monolayer of Si atoms. This plane is perpendicular to the rotoreflection axis (S_4 point group).

The so built *t*- and *a*-based symmetric double interfaces were partially reoptimized using the SIESTA code,[53] which is based on the LCAO method. Trouillier-Martin (TM) pseudopotentials were employed.[54] Exchange-correlation was calculated within the GGA, using the Perdew-Becke-Ernzerhof (PBE) potential.[55,56] As before, a $6\times1\times6$ Monkhorst-Pack *k*-point sampling scheme was employed.[50] Other relevant calculation parameters were the use of the Single-Zeta plus polarization (SZP) basis set, a 140 Ry cutoff mesh for the solution of the Poisson equation, and convergence of atomic positions achieved for residual forces below 0.05 eV/Å.

VASP and SIESTA bulk calculations of anatase and tetragonal HfO_2 give the same ordering for the lowest energy structure with *t*-HfO_2 more stable than *a*-HfO_2 by 160 meV/unit formula obtained with VASP and 98 meV/unit formula obtained with SIESTA. To reproduce the strain condition of the HfO_2 slabs in our NSOI models, we repeated the bulk oxide calculations using the Si unit cell vectors along one unit cell plane and dimensioned the orthogonal unit cell vector such as to minimize the total energy of the oxide. Mechanical stress at the plane of the interface is obtained from the ratio $1-a_{\mathrm{fit}}/a_{\mathrm{relaxed}}$, where a_{relaxed} represents the hafnia relaxed lattice parameter, while a_{fit} is the lattice parameter of the oxide matching the experimental Si unit cell vector in the plane of the interface (3.8403 Å). The calculated lattice parameter for *a*-HfO_2 is 3.983 Å with PW/GGA and 3.942 Å with PW/LDA, and for *t*-HfO_2 it is 3.569 Å with PW/GGA and 3.509 Å with PW/LDA. The resulting mechanical stress is tensile for *t*-HfO_2 at GGA and LDA levels (7.6% and 9.4%, respectively) and compressive for *a*-HfO_2 (3.3% and 2.5%, respectively). For the strained bulk polymorphs, VASP still ranks *t*-HfO_2 as the lowest energy structure while stressed *a*-HfO_2 collapses into the tetragonal phase. At odds with bulk results, a different behavior is observed for the slab structures. Due to the close proximity of the *a*-HfO_2 lattice parameters to that of experimental Si, relaxing the *t*-NSOI with VASP results in *a*-NSOI. This is not necessarily the case in experiments where interface stress relaxation may take place through a number of pathways not considered in the present work, among them the absence of the artificial periodic boundary conditions imposed by the calculation method, interface defects, and a thicker IL separating the channel from the dielectric. Therefore, to retain its tetragonal crystal structure in *t*-NSOI, only the positions of the atoms in the interface region between Si and *t*-HfO2 (i.e., one Si, one O, and one Hf monolayer adjacent to the interface) were relaxed with VASP while the other atoms were kept in their fixed bulk positions (only scaled according the Si unit-cell vectors as explained before). For *a*-NSOI all the atom positions were relaxed with VASP.

B. Transport calculation

For transport calculation, both *a*- and *t*-NSOI models were replicated along the transport direction (z) by a factor of 8. Using the SIESTA code, converged total energies were obtained for these 296 atom structures, respectively, employing seven *k*-points along the short x direction and the SZP basis set. As far as transport is concerned, the accuracy of SZP is very close to that of Double-Zeta plus polarization (DZP), the most complete SIESTA basis set available, yet it is more efficient in the use of computer resources. The SZP and DZ results are also comparable, however SZP yields better band offsets, which is important for isolating transport in the channel from transport in the oxide. This issue is discussed in more detail below.

The output Hamiltonian matrix of the SIESTA calculation was then used to obtain the transmission function using nonperturbative elastic-scattering theory.[34] The current was calculated using the Fermi golden rule with the matrix elements of the scattering operator $T(E,V)$ obtained from the solution of the Lippmann-Schwinger equation, which is accurate to all orders.[34] In the presence of an external bias the scattering operator is a function of both the energy and the bias. Here we adopt the rigid band approximation $T(E,V)=T(E+1/2V)$, which implies that the electronic band structure is not affected by the external electric field. In this case the electric current at low temperature is given by[57]

$$I(V)=\int_{E_f-0.5V}^{E_f+0.5V}T(E)dE, \tag{1}$$

where E_f is the Fermi energy. This approximation works well for small external electric field compared with the atomic electric field. This is indeed the case in the present work where a maximum bias of ~1 V (source-drain bias difference) is applied over a distance of ~15 Å (channel length) implying an external electric field of 0.07 V/Å, which is 2–3 orders of magnitude smaller than typical atomic electric fields.

A number of important scattering processes have been neglected in our transport model. Among them it is worth mentioning phonon scattering and Coulomb screening in the channel.[58] However, it is well known that under strong trans-

TABLE I. Structural parameters calculated for the anatase (*a*-NSOI) and tetragonal (*t*-NSOI) HfO_2/Si interfaces, and for the inner (inn) regions. Corresponding atom numbers are indicated in Fig. 2.

	Bond angles (deg)						Bond lengths (Å)		
	O-Si-Si	O-Si-O	Si-Si-Si	Hf-O-Si	Hf-O-Hf	O-Hf-O	Si-O	Si-Si	Hf-O
a-NSOI	$\alpha_{1-7-2}=98.2$	$\alpha_{1-7-14}=153.9$	$\alpha_{2-1-3}=109.6$	$\alpha_{8-1-9}=110.4$	$\alpha_{9-8-9'}=139.6$	$\alpha_{9-8-7}=69.8$	$d_{1-14}=1.97$	$d_{1-2}=2.35$	$d_{7-9}=2.08$
	$\alpha_{1-8-2}=123.5$	$\alpha_{1-8-14}=77.2$	$\alpha_{3-2-4}=110.3$	$\alpha_{7-1-9}=103.1$		$\alpha_{9-8-15}=139.6$	$d_{1-7}=1.97$	$d_{2-3}=2.37$	$d_{9-8}=2.04$
						$\alpha_{9-8-13}=84.2$	$d_{1-8}=1.83$		$d_{9-10}=2.05$
						$\alpha_{9-8-10}=100.2$			$d_{9-13}=2.05$
						$\alpha_{9-7-10}=110.7$			
			$\alpha_{inn}=110.4$		$\alpha_{inn}=138.4$	$\alpha_{inn}=137.4$		$d_{inn}=2.38$	$d_{inn}=2.08$
					137.8	73.7			2.13
					107.2	147.6			2.17
					106.4	85.1			2.04
					105.6	108.4			
t-NSOI	$\alpha_{1-7-2}=97.5$	$\alpha_{1-8-7}=97.9$	$\alpha_{1-2-3}=102.5$	$\alpha_{8-1-9}=98.0$	$\alpha_{9-8-9'}=117.7$	$\alpha_{9-7-14}=67.1$	$d_{1-8}=1.77$	$d_{1-2}=2.42$	$d_{9-14}=2.27$
	$\alpha_{1-8-2}=143.4$		$\alpha_{3-2-4}=109.7$	$\alpha_{7-1-9}=71.4$	$\alpha_{10-9-13}=76.1$	$\alpha_{9-7-8}=56.5$	$d_{1-7}=1.72$	$d_{2-3}=2.36$	$d_{9-8}=2.06$
				$\alpha_{8-1-9'}=143.7$	$\alpha_{10-9-11}=102.3$	$\alpha_{9-14-8}=117.7$			$d_{9-7}=2.22$
					$\alpha_{13-11-9}=108.7$	$\alpha_{9-10-13}=76.1$			$d_{9-10}=2.22$
						$\alpha_{11-10-13}=72.3$			$d_{9-10'}=2.15$
						$\alpha_{9-10'-9'}=122.7$			$d_{9-13}=2.07$
			$\alpha_{inn}=109.7$		$\alpha_{inn}=121.2$	$\alpha_{inn}=121.2$		$d_{inn}=2.35$	$d_{inn}=2.21$
					72.8	107.3			2.41
					111.3	72.8			2.20
					107.3	105.6			

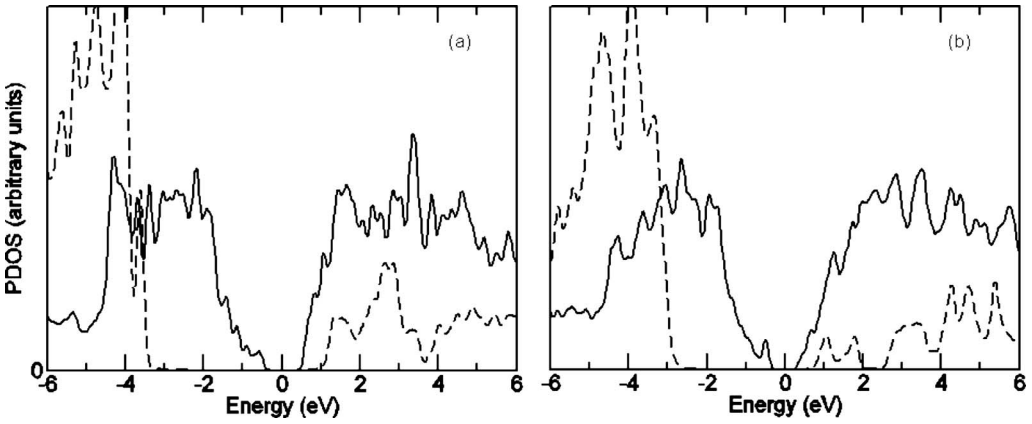

FIG. 3. Band offsets calculated for *a*- and *t*-NSOI using projected density of states onto Si and O atoms far away from the interfaces.

versal fields interface roughness is the leading scattering mechanism.[59] Because our NSOI is so thin, the carriers are tightly confined between the two oxide slabs thus encountering a high degree of confinement typical of strong transversal fields.[60] A detailed description of our implementation is presented elsewhere.[35]

III. RESULTS

The main difference between the interfaces of the *t*-NSOI and *a*-NSOI structures is the Si coordination, which is fourfold in the former and fivefold in the latter, revealing the higher ionic character of the *a*-NSOI interfaces. In *t*-NSOI tensile stress influences the coordination of Hf, reducing it from its bulk sevenfold value to sixfold at the interface giving rise to Hf-O elongated bonds ranging from 2.07 to 2.27 Å. Oxygen atoms are two- and threefold coordinated at the interface of *t*-NSOI. Differently, in *a*-NSOI the Hf coordination remains sixfold in the bulk and interface regions; this structure is highly symmetric, with all the O atoms threefold coordinated. Here, all the Hf-O distances, ranging from 2.04 to 2.08 Å, are close to their experimental value (2.03–2.20 Å).[61] The shorter Hf-O bonds in *a*-NSOI confirm its higher ionic character. The calculated Si-O bond lengths at the interfaces are 1.72 Å for the bond between Si and the twofold coordinated interface O atoms and 1.77 Å for the bond between Si and the threefold coordinated interface O atoms in *t*-NSOI (Fig. 2). For *a*-NSOI, they are 1.83 Å for the Si-O bond normal to the plane of the interface, and 1.97 Å for the Si-O bond in the plane of the interface (Fig. 2). These Si-O interface bonds are longer than the calculated value (1.60 Å) for Si-O in β-cristobalite,[51] and are also longer than the experimental values reported for both vitreous silica (1.61 Å) (Ref. 62) and for α-, β-, and high-*T* cristobalite phases (1.62 Å).[63,64] Si-Si bond lengths at the interface are 2.42 and 2.49 Å for *t*-NSOI, while 2.35 Å for *a*-NSOI. Table I summarizes all relevant structural parameters calculated for the two structures.

To gain insight on the degree of confinement during carrier transport for the two systems in Fig. 3, we compare the band offsets obtained for the two interfaces using the projected density of states (PDOS) onto Si and O atoms far away from the interfaces. For *a*-NSOI the Si band gap is 1.1 eV and the *a*-HfO_2 band gap is 5.3 eV, with a valence band offset (VBO) of ~3.5 eV and a conduction-band offset (CBO) of ~0.7 eV. For *t*-NSOI the Si band gap is ~0.7 eV, smaller than for *a*-NSOI due to the presence of interface states in the Si band gap (see discussion below), and the *t*-HfO_2 band gap is 4.3 eV, with a VBO of ~3.0 eV and a CBO of ~0.6 eV. Since the bulk Si, strained *a*-HfO_2, and strained *t*-HfO_2 band gaps obtained with the SZP basis set, the same used in the stack calculations, are 0.7, 4.3, and 2.60 eV, respectively, it is clear that the confinement effect is quite strong in such narrow channel and in the oxide. The underestimation of the calculated band gap is a common shortcoming of DFT which also affects the band offsets.[65] Here, because the confinement effect is so strong, a direct comparison of our calculated band offsets with experimental data would be meaningless. Nevertheless, they set a limit to the energy window used for the calculation of the transmission function. Indeed, to analyze individual carrier transport the energy window must be twice the minimum between the band gap and the band offset to avoid the onset of minority carrier transport and transport in the oxide, respectively. For example, for hole transport calculation at the Si valence-band edge (VBE) of *a*-NSOI, the energy window can be as wide as 2.2 eV (twice the Si band gap since it is smaller than the *a*-NSOI VBO). A wider window would reach the Si conduction-band edge (CBE) and mix hole and electron transport at a bias higher than 2.2 V. Similarly, for electron transport at the Si CBE of *a*-NSOI, the energy window can be only 1.4 eV wide (1.2 eV for *t*-NSOI), which is twice the *a*-NSOI CBO.

To investigate the presence of interface states in the Si gap, in Fig. 4 we show the PDOS taken along the Si slab, which indicates a clean band gap for *a*-NSOI, even for Si atoms at the interface. On the other hand, the *t*-NSOI PDOS reveals the presence of interfacial states that penetrate the Si channel. These interfacial states are mostly localized at the VBE, even if some states are detected also at the CBE. The origin of these *p*-like states at the Si VBE is strain, which at the interface stretches the Si-Si bonds in *t*-NSOI. Indeed, while the Si-Si distance in the bulk region of the Si channel is 2.36 Å, at the interface it is 2.49 Å (see Fig. 2), an increase in 5.5%. In *a*-NSOI, on the other hand, the Si-Si bond

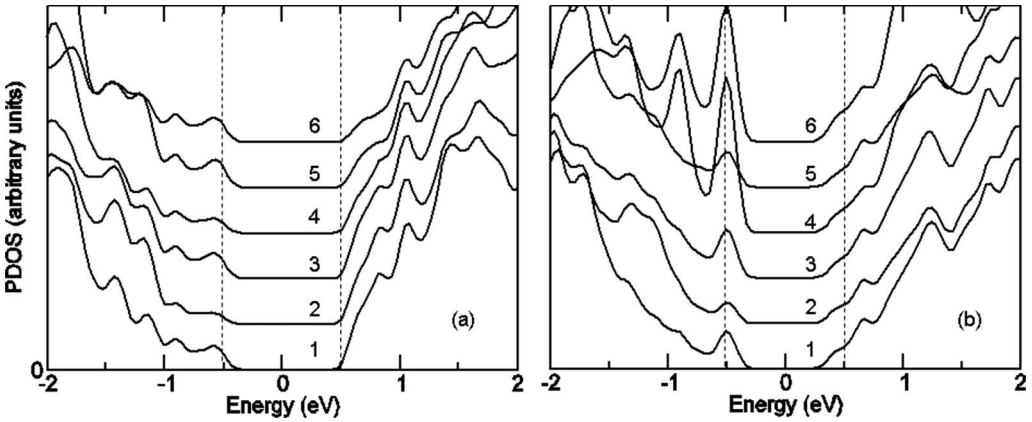

FIG. 4. Projected density of states onto silicon atoms numbered 1–6 as shown in Fig. 2. (a) While the band gap is clean in the anatase-based structure, (b) interface states penetrate the silicon band gap all the way to the center of the silicon slab in the tetragonal-based structure. PDOS lines have been shifted for clarity. Zero of energy at the Fermi level. Energy broadening is 100 meV.

length varies much less, from 2.38 Å in the middle of the Si channel to 2.35 Å at the interface, a change in only 1.3%. PDOS taken on the interface Si atoms shows that the band-edge peaks associated with interface states are localized on the interface Si atoms (not shown). The presence of interface scattering states in the Si band gap in *t*-NSOI is expected to lower the channel mobility.

To check this hypothesis, in Fig. 5 we compare the transmission functions obtained for *a*-NSOI and *t*-NSOI at 0 V gate bias, which shows that even though transmission occurs earlier at the Si band edges in *t*-NSOI than in *a*-NSOI, at higher absolute values of the energy, especially for electrons (energy >0), it becomes higher for *a*-NSOI. This result is counter intuitive: at the band edges, where the interface states are localized, a residual transmission in *t*-NSOI takes place through those same states. This residual transmission is thus higher than in the absence of interface states in *a*-NSOI, where transmission is zero as there are no states in the energy-band gap to transmit carriers. However, at energies higher (lower) than the CBE (VBE), those interface states scatter the carriers, lowering their transmission. Notice that the onsets of transmission correspond to the location of the Si band edges shown in Figs. 3 and 4.

Figure 6 shows the calculated electron and hole currents and conductances for the two types of interfaces as function of the source-drain bias and 0 V gate bias. For these calculations the Fermi level was placed at the Si CBE (VBE) for electron (hole) transport calculation, mimicking the effect of channel doping, and an energy window for transmission calculation was opened around the Fermi level (the window width is twice the source-drain bias).[35] This procedure shifts the onsets of electron and hole transmissions for the two interfaces to the same energy value, thus avoiding the difficulty of comparing transmission values with different onset energies. Electron current in *t*-NSOI is now clearly lower than in *a*-NSOI, showing that the interface states in *t*-NSOI are bad carrier transmitters. Electron current in *a*-NSOI is almost four times larger than in *t*-NSOI at 1 V source-drain bias. Hole current is 2.3 times lower than electron current in *a*-NSOI, as expected from the lower hole mobility in Si and also slightly lower than hole current in *t*-NSOI in the bias range investigated. This result indicates that the interface states near the Si VBE are better hole transmitters than the interface states near the Si CBE are electron transmitters. Moreover, the higher density of the interface states near the VBE (Fig. 4) also plays a role in enhancing hole current (Figs. 5 and 6). However, notice that the hole current behavior in *t*-NSOI is ohmic, at least in the bias range considered. Therefore hole current in *a*-NSOI may be higher than in

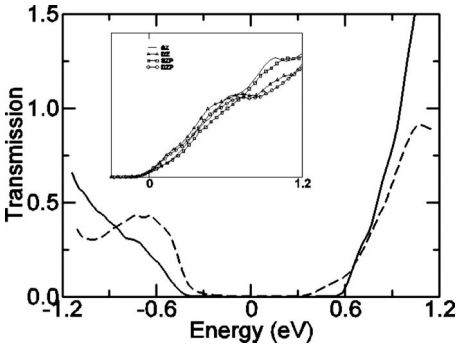

FIG. 5. Transmission function for *a*-NSOI (solid) and *t*-NSOI (dashed) structures. Zero of energy at the Fermi level. Energy broadening is 50 meV. The inset shows the weak dependence of the transmission function on bases sets for *a*-NSOI.

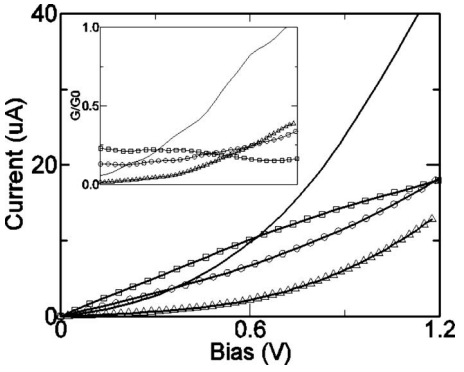

FIG. 6. Electron and hole current and conduction (inset, in units of the quantum of conductance $G_0^{-1}=R_0=12.9$ kΩ) in the silicon channel as function of source-drain bias. Solid (circle): electron (hole) in *a*-NSOI; triangle (square): electron (hole) in *t*-NSOI.

t-NSOI at higher bias. The ohmic behavior for holes in *t*-NSOI is shown clearly in the carriers conductance plot (Fig. 6), where the hole conductance is quite flat and is surpassed by the hole conductance in *a*-NSOI at ~0.7 V. The hole conductance in *a*-NSOI is nearly constant at low bias (below 0.3 V) indicating some impact of the interface on the hole transmission, though to a lower extent than in *t*-NSOI.

IV. CONCLUSIONS

In this paper we have focused our attention on the impact of the crystal structure of two oxide polymorphs, anatase (*a*-) and tetragonal (*t*-) HfO_2 on the transport properties of ultrathin Si channel in the SOI configuration, $HfO_2/Si/HfO_2$. Our study is based on first-principles calculations of electronic and transport properties of atomistic models of SOI devices. We have found that while the tetragonal polymorph creates scattering states, mostly near the Si band valence-band edge, through the presence of stretched Si-Si bonds at the interface, the anatase polymorph, being a better lattice match to Si, does not create interface states in the Si band gap. As a result electron transport is more efficient for Si in contact with *a*-HfO_2 than in contact with *t*-HfO_2. For holes, transport is slightly more efficient for Si in contact with *t*-HfO_2. However, the ohmic hole transport characteristics found for the Si/*t*-HfO_2 interface suggests lower hole current at higher source-drain bias than in Si/*a*-HfO_2. We have also found that interface states can be harmful in two ways: by creating a possible source-drain leakage path in the subthreshold region, thus lowering the on/off current ratio, and by degrading mobility in the channel.

The many interface model assumptions used in this work make our conclusions rather qualitative. However, they raise an important point regarding the impact of the HfO_2 grain structure (or of any other polycrystalline oxide) on the mobility of carriers in the channel. Even if the grains are all in the same phase and even if all interface point defects are appropriately saturated, the grains different orientations may stress the Si atoms at the interface, generating interface states that spread several monolayers in the bulk of the channel. Carriers would then be scattered differently along the channel as they move from source to drain. Our calculations have shown that due to interface stress, an increase in 5.5% of the Si-Si bond lengths near the interface with respect to their bulk values in our model causes a drop in the electron current of almost four times at 1 V source-drain bias, but has little impact on the hole current. These results may explain the measured electron mobility degradation when the SiO_2 layers naturally formed between Si and HfO_2 are made very thin. Therefore, to minimize mobility degradation and to enhance process reproducibility by reducing the variation in carrier mobility between transistors, steps should be taken to alleviate interface stress. This may be accomplished through oxide amorphization, at least near the interface, or by the implementation of an amorphous buffer layer between HfO_2 and Si.

ACKNOWLEDGMENTS

The authors are thankful to D. Thober for his support and motivation, and M. Ribeiro, Jr. for stimulating discussions. They also want to thank H. Nakamura and H. Kamisaka of the Department of Chemical System Engineering, Graduate School of Engineering, The University of Tokyo, for their support and F. Mercuri of the CNR-ISTM, c/o Università di Perugia for useful suggestions. G.G. is grateful to "21st Century COE Program" for financial support. This research was supported by a Grant-in-aid for the global COE program.

*giacomo@tcl.t.u-tokyo.ac.jp
†fonseca@vonbraunlabs.com.br
‡korkin@nanoandgiga.com
§yamasita@chemsys.t.u-tokyo.ac.jp

[1] S. Cristoloveanu and S. S. Li, *Electrical Characterization of SOI Materials and Devices* (Kluwer, Dordrecht, 1995).
[2] G. E. Moore, Proc. IEEE **86**, 82 (1998) (reprint); P. M. Zeitzoff, J. M. Hutchby, G. Bersuker, and H. R. Huff, in *Nano and Giga Challenges in Microelectronics*, edited by J. Greer, A. Korkin, and J. Labanowski (Elsevier, Amsterdam, 2003).
[3] J. Robertson, Rep. Prog. Phys. **69**, 327 (2006).
[4] J. Tang, J. Fabbri, R. D. Robinson, Y. Zhu, I. P. Herman, M. L. Steigerwald, and L. E. Brus, Chem. Mater. **16**, 1336 (2004).
[5] J. E. Lowther, J. K. Dewhurst, J. M. Leger, and J. Haines, Phys. Rev. B **60**, 14485 (1999).
[6] O. Ohtaka, H. Fukui, T. Kunisada, T. Fujisawa, K. Funakoshi, W. Utsumi, T. Irifune, K. Kuroda, and T. Kikegawa, Phys. Rev. B **63**, 174108 (2001).
[7] A. Jayaraman, S. Y. Wang, S. K. Sharma, and L. C. Ming, Phys. Rev. B **48**, 9205 (1993).
[8] J. M. Leger, A. Atouf, P. E. Tomaszewski, and A. S. Pereira, Phys. Rev. B **48**, 93 (1993).
[9] J. M. Leger, P. E. Tomaszewski, A. Atouf, and A. S. Pereira, Phys. Rev. B **47**, 14075 (1993).
[10] M. T. Currie, C. W. Leitz, T. A. Langdo, G. Taraschi, E. A. Fitzgerald, and D. A. Antoniadis, J. Vac. Sci. Technol. B **19**, 2268 (2001).
[11] J.-P. Colinge, *Silicon-on-Insulator Technology: Materials to VLSI*, 3rd ed. (Birkhäuser, 2004).
[12] G. He, M. Liu, L. Q. Zhu, M. Chang, Q. Fang, and L. D. Zhang, Surf. Sci. **576**, 67 (2005).
[13] M.-S. Kim, Y.-D. Ko, T.-H. Moon, J.-M. Myoung, and I. Yun, Microelectron. J. **37**, 98 (2006).
[14] V. Fiorentini and G. Gulleri, Phys. Rev. Lett. **89**, 266101 (2002).
[15] A. S. Foster, F. Lopez Gejo, A. L. Shluger, and R. M. Nieminen, Phys. Rev. B **65**, 174117 (2002).
[16] A. S. Foster, V. B. Sulimov, F. Lopez Gejo, A. L. Shluger, and R. M. Nieminen, Phys. Rev. B **64**, 224108 (2001).
[17] J. K. Dewhurst and J. E. Lowther, Phys. Rev. B **57**, 741 (1998).
[18] F. Birch, J. Geophys. Res. **83**, 1257 (1978).
[19] A. Pasquarello, M. S. Hybertsen, and R. Car, Phys. Rev. Lett. **74**, 1024 (1995).

[20] A. Pasquarello, M. S. Hybertsen, and R. Car, Phys. Rev. B **53**, 10942 (1996).
[21] A. Korkin, J. C. Greer, G. Bersuker, V. V. Karasiev, and R. J. Bartlett, Phys. Rev. B **73**, 165312 (2006).
[22] A. A. Demkov and O. F. Sankey, Phys. Rev. Lett. **83**, 2038 (1999).
[23] P. W. Peacock and J. Robertson, Phys. Rev. Lett. **92**, 057601 (2004).
[24] P. W. Peacock, K. Xiong, K. Y. Tse, and J. Robertson, Phys. Rev. B **73**, 075328 (2006).
[25] R. Puthenkovilakam, E. A. Carter, and J. P. Chang, Phys. Rev. B **69**, 155329 (2004).
[26] M. V. Fischetti and S. E. Laux, Phys. Rev. B **48**, 2244 (1993).
[27] H. Kothari, A. Ramamoorthy, R. Akis, S. M. Goodnick, D. K. Ferry, J. L. Reno, and J. P. Bird, J. Appl. Phys. **103**, 013701 (2008).
[28] Li-Na Zhao, Xue-Feng Wang, Zhen-Hua Yao, Zhu-Feng Hou, Marcus Yee, Xing Zhou, Shi-Huan Lin, and Teck Seng Lee (unpublished).
[29] K. Hess, I. C. Kizilyalli, and J. W. Lyding, IEEE Trans. Electron Devices **45**, 406 (1998).
[30] D. J. Frank, R. H. Dennard, E. Nowak, P. M. Solomon, Y. Taur, and H.-S. P. Wong, Proc. IEEE **89**, 259 (2001).
[31] S. E. Laux, A. Kumar, and M. V. Fischetti, IBM Research Report No. RC22539 (W0208-025) (2002).
[32] E. Gnani, S. Reggiani, M. Rudan, and G. Baccarani, IEEE Trans. Nanotechnol. **6**, 90 (2007).
[33] P. Hohenberg and W. Kohn, Phys. Rev. **136**, B864 (1964); W. Kohn and L. J. Sham, *ibid.* **140**, A1133 (1965).
[34] J. J. Sakurai, *Modern Quantum Mechanics* (Addison-Wesley, Reading, 1994).
[35] L. R. C. Fonseca, A. A. Demkov, and A. Knizhnik, Phys. Status Solidi B **239**, 48 (2003).
[36] M. Ribeiro, Jr., L. R. C. Fonseca, and A. A. Korkin (unpublished).
[37] P. Caplan, E. Poindexter, B. Deal, and R. Razouk, J. Appl. Phys. **50**, 5847 (1979).
[38] A. Stirling, A. Pasquarello, J.-C. Charlier, and R. Car, Phys. Rev. Lett. **85**, 2773 (2000).
[39] E.-C. Lee, Phys. Rev. B **77**, 104108 (2008).
[40] J. P. Perdew, J. A. Chevary, S. H. Vosko, K. A. Jackson, M. R. Pederson, D. J. Singh, and C. Fiolhais, Phys. Rev. B **46**, 6671 (1992).
[41] J. P. Perdew and Y. Wang, Phys. Rev. B **45**, 13244 (1992).
[42] J. P. Perdew and A. Zunger, Phys. Rev. B **23**, 5048 (1981).
[43] Vienna *ab initio* simulation package (VASP), version 4.5.8, http://cms.mpi.univie.ac.at/vasp/, and references therein.
[44] D. Vanderbilt, Phys. Rev. B **41**, 7892 (1990)
[45] G. Kresse and J. Hafner, J. Phys.: Condens. Matter **6**, 8245 (1994).
[46] D. M. Ceperley and B. J. Alder, Phys. Rev. Lett. **45**, 566 (1980).
[47] K. Burke, J. P. Perdew, and Y. Wang, in *Electronic Density Functional Theory: Recent Progress and New Directions*, edited by J. F. Dobson, G. Vignale, and M. P. Das (Plenum, New York, 1998).
[48] J. P. Perdew, in *Electronic Structure of Solids '91*, edited by P. Ziesche and H. Eschrig (Akademie, Berlin, 1991).
[49] J. P. Perdew, J. A. Chevary, S. H. Vosko, K. A. Jackson, M. R. Pederson, D. J. Singh, and C. Fiolhais, Phys. Rev. B **46**, 6671 (1992).
[50] H. J. Monkhorst and J. D. Pack, Phys. Rev. B **13**, 5188 (1976).
[51] G. Giorgi, A. Korkin, and K. Yamashita, Comput. Mater. Sci. **43**, 930 (2008).
[52] A. Debernardi, C. Wiemer, and M. Fanciulli, Phys. Rev. B **76**, 155405 (2007).
[53] Spanish initiative for electronic simulations with thousands of atoms (SIESTA), version 2.0, http://www.uam.es/departamentos/ciencias/fismateriac/siesta, and references therein.
[54] N. Troullier and J. L. Martins, Phys. Rev. B **43**, 1993 (1991).
[55] J. P. Perdew, K. Burke, and M. Ernzerhof, Phys. Rev. Lett. **77**, 3865 (1996).
[56] J. P. Perdew, K. Burke, and M. Ernzerhof, Phys. Rev. Lett. **78**, 1396 (1997).
[57] Supryio Datta, *Electronic Transport in Mesoscopic Systems* (Cambridge University Press, Cambridge, England, 1997).
[58] M. V. Fischetti and S. E. Laux, J. Appl. Phys. **89**, 1205 (2001).
[59] S. E. Laux, A. Kumar, and M. V. Fischetti, IEEE Trans. Nanotechnol. **1**, 255 (2002).
[60] F. Gámiz, J. B. Roldán, J. A. López-Villanueva, F. Jiménez-Molinos, and J. E. Carceller, Microelectron. Eng. **59**, 423 (2001).
[61] J. Wang, H. P. Li, and R. Stevens, J. Mater. Sci. **27**, 5397 (1992).
[62] R. L. Mozzi and B. E. Warren, J. Appl. Crystallogr. **2**, 164 (1969).
[63] M. T. Dove, D. A. Keen, A. C. Hannon, and I. P. Swainson, Phys. Chem. Miner. **24**, 311 (1997).
[64] D. Hatch and S. Ghose, Phys. Chem. Miner. **17**, 554 (1991).
[65] S. B. Zhang, M. L. Cohen, S. G. Louie, D. Tománek, and M. S. Hybertsen, Phys. Rev. B **41**, 10058 (1990).